Microporous structure and enhanced hydrophobicity in methylated SiO_2 for molecular separation†

Hessel L. Castricum,*[ab] Ashima Sah,[b] Marjo C. Mittelmeijer-Hazeleger,[a] Cindy Huiskes[b] and Johan E. ten Elshof[b]

Received 18th July 2006, Accepted 13th December 2006
First published as an Advance Article on the web 15th January 2007
DOI: 10.1039/b610311a

Methylated microporous silica with high thermal stability and tuneable hydrophobicity was obtained by acid-catalysed sol–gel hydrolysis and condensation of mixtures of tetraethylorthosilicate (TEOS) and methyltriethoxysilane (MTES). The gels exhibited a trend towards smaller ultramicropores with increasing methyl content, while in addition some supermicropores were formed with sizes of around 2 nm. For low MTES concentration, dilution prior to gelation and ageing resulted in materials with clearly smaller ultramicropores, whereas only a minor effect of dilution on structure was found at high MTES concentration. The small ultramicropore size in 'diluted' materials can be associated with a higher extent of condensation of mainly TEOS monomers. Stable structures formed from MTES in an early stage of synthesis may explain the particular micropore structure of MTES-rich gels. With increasing methyl content and with dilution of the sol, the affinity of the surface to water was strongly decreased. The applicability of microporous silica in wet atmospheres may thus be improved by methylation, and their pore structure modified by adaptation of the recipe, which would be highly relevant for industrial gas and liquid separation by inorganic membranes.

1. Introduction

Microporous materials are an important class of materials with a vast potential of applications in ion exchange, gas separation, adsorption, fine chemical synthesis, oil refining and molecular sieving (*e.g.* desiccation). Sol–gel synthesis has emerged as an extremely versatile technique for preparation of high-purity microporous materials with well-controlled physical and chemical properties. As structures are formed under conditions of non-thermodynamic equilibrium, it is the most suitable route for synthesis of highly porous and amorphous materials, which would otherwise be unattainable. Silica is by far the oldest and best studied of the sol–gel systems. The first alkoxysilanes were prepared as early as 1844,[1] but it took until the late 1910s until the first solid structures were produced from these agents with the sol–gel technique.[2] A myriad of applications are associated with adsorption on porous silica, including chromatography, heterogeneous catalysis and membrane technology. Characteristics that contribute to the applicability of silica include chemical inertness and high mechanical and thermal stability. Limitations are however set by the vast number of steps involved in sol–gel synthesis, reproduction involving full control over all preparation parameters. In addition, precursors are usually expensive and preparation is very time-consuming. Consequently, practical application of this approach is most successful for the synthesis of non-porous and ultramicroporous materials (pore diameter <0.6 nm) in small volume quantities and for advanced applications, such as thin layers, coatings and membranes.

Defect-free thin film silica membranes, which are the main scope of this study, have been known since the late 1980s,[3,4] although the first idea of making such membranes from $Si(OR)_4$ was put forward as early as 1928.[5] They are typically prepared by acid-catalysed hydrolysis and condensation of alkoxysilanes, which gives rise to the formation of an initially slightly branched network. After ageing, drying and calcination, a microporous structure with a narrow pore size distribution is obtained. For pore sizes <1 nm, the transport of small molecules is considerably faster than that of larger ones. Inorganic membranes have significant advantages over organic polymer membranes with respect to performance (selectivity and flux) and chemical and thermal stability. For this reason, they are envisaged to play a major role in the bio- and process industry for pervaporation, liquid separation and gas separation, including dehydrogenation of hydrocarbons and purification of H_2.[4,6,7] However, state-of-the-art microporous silica membranes suffer from extensive water adsorption due to the hydrophilic nature of the silica surface. This is related to the large number of hydroxyl groups that typically occupy the surface and are responsible for strong H-bonding with water.[8,9] In wet atmospheres, capillary condensation of water and pore blockage thus lead to a decreased permeability of other molecules. In addition, interaction of the membrane with water from process streams can result in serious degradation phenomena due to dissociation of Si–O–Si bonds,

[a]*Van't Hoff Institute for Molecular Sciences, Faculty of Science, Universiteit van Amsterdam, Nieuwe Achtergracht 166, 1018 WV Amsterdam, The Netherlands. E-mail: castric@science.uva.nl; Fax: +31 20 5255604; Tel: +31 20 5256493*
[b]*Inorganic Materials Science, Department of Science and Technology, Universiteit Twente, MESA+ Institute for Nanotechnology, P.O. Box 217, 7500 AE Enschede, The Netherlands*
† Electronic supplementary information (ESI) available: scanning electron micrographs of silica surfaces. See DOI: 10.1039/b610311a

especially at higher temperatures. For application in membranes and in chromatography, this leads to impairment of the separation properties, setting strong limitations on the operating conditions. These limitations should be overcome to enable large-scale industrial application, which may generate large cost and energy savings.

The affinity of silica to water can be decreased strongly by reducing the number of vicinal (adjacent) OH groups that are responsible for the strongest hydrophilic interaction.[8–10] In fact, nearly all surface hydroxyls can be removed effectively by a thermal treatment at 1073 K, with only very slow subsequent rehydroxylation upon exposure to water.[8] However, this treatment also leads to sintering and thus to almost complete loss of porosity and of the percolative micropore structure that is needed for the desired separation properties. Adsorption of water can also be suppressed if the hydroxyl groups are replaced by hydrolytically stable groups with a hydrophobic character, such as $-CH_3$. The low polarity of this group implies a lower affinity to water. For microporous materials, a simple post-modification treatment by grafting that can be carried out for materials with pore diameters down to 2 nm is not feasible due to transport constraints of the silane agents into the pores.[11] The only available approach is thus to incorporate this organic functionality by *in situ* hydrolysis and condensation of alkoxide precursors with hydrophobic side groups, such as organoalkoxysilanes.[7,12] This method has also been applied successfully for the preparation of hydrophobic aerogels and silica glass surfaces.[13] It is essential to define the factors that determine the structure and surface chemistry of microporous silica for controlled manufacture and optimisation of hydrophobic membranes. A major challenge herein is acquiring information on the pore structure, as the sub-nm scale troubles proper characterisation.

In the present study, a series of unsupported silica materials were prepared with different methyltriethoxysilane (MTES) : tetraethylorthosilicate (TEOS) ratios, based on a recipe that resulted earlier in the successful formation of a hydrophobic membrane with high hydrothermal stability.[7,12] The disordered, amorphous structure of these membranes guarantees an intrinsically low number of defects. The acid hydrolysis and condensation rates of MTES are higher than those of TEOS,[14] the isoelectric point is at a higher pH, and MTES has a smaller number of reactive ethoxy groups. Therefore, it can be expected that a different type of network is formed with MTES than from pure TEOS, for which indications have also been found by De Vos *et al.*[12] and Da Costa *et al.*[15] Hydrophobicity and microstructure were studied upon variation of the methyl group concentration and of the degree of dilution with ethanol. As dilution leads to lower reaction kinetics, an effect on network formation during gelation and ageing is anticipated. Although slight differences in structure with supported films may occur, unsupported membrane materials are studied here as these allow more extensive and accurate structural characterisation. Thermal stability and affinity to water adsorption were assessed by temperature programmed oxidation–mass spectrometry (TPO-MS). Hydrophobicity was also determined in terms of the 3-phase contact angle with water. The internal pore structure was studied by various adsorption methods, *i.e.* N_2, CO_2 and C_2H_2 physisorption, in combination with He and Hg pycnometry.

2. Experimental

2.1. Materials preparation

The recipes for the preparation of both conventional (TEOS-based) silica and MTES-modified silica were based on recipes that have been proven to result in selective membranes.[12,16] TEOS (99.999% pure), MTES (99% pure) and dry ethanol were obtained from Aldrich. For unmodified materials, TEOS was mixed with ethanol in equal volumetric amounts and placed in an ice bath to avoid premature (partial) hydrolysis. A mixture of nitric acid and doubly distilled water was added dropwise under vigorous stirring. After addition, the reaction mixture was heated for 3 h at 333 K in a water bath under continuous stirring. The reaction mixture had a (based on starting compounds) TEOS : ethanol : water : acid molar ratio of 1 : 3.8 : 6.4 : 0.085 according to this recipe of silica sol preparation.[16] For modified materials (25, 50, 75 and 100 mol% MTES, respectively), MTES was mixed with ethanol in equal volumetric amounts and added in an ice bath to the standard TEOS-based reaction mixture that had refluxed for 2.75 h. This MTES–TEOS-based reaction mixture was heated at 333 K for another 15 min. For pure MTES-based materials, the total reaction time at 333 K was consequently only 15 minutes. For 50% MTES, the mixture had a (based on starting compounds) MTES : TEOS : ethanol : water : acid molar ratio of 1 : 1 : 7.6 : 6.4 : 0.085. The other modified materials had similar Si : H_2O and Si : EtOH ratios. The differences in reaction time of the precursors were applied in view of the higher reactivity of MTES. This procedure has earlier enabled synthesis of composite materials with microporous structures suitable for application as a membrane.[12]

Subsequently, the reacted mixture was cooled and was then either left undiluted or was diluted 19-fold with ethanol. 60 ml of sol was allowed to dry in a 10 cm diameter Petri dish at room temperature, and silica gel flakes were obtained overnight. For undiluted sols, the thickness of the formed gels was about 2–4 mm, and for diluted ones it was about 0.1–0.3 mm. After drying, the materials were calcined for 3 h in N_2 (99.999% pure) at 673 K using heating and cooling rates of 0.5 K min^{-1}.

2.2. Materials characterisation

For assessing the amount of adsorbed water and the ignition temperature of the organic fraction, thermogravimetric analysis–mass spectrometry (TGA-MS) was carried out in a Setaram TG 85 thermobalance. During heating of the materials in synthetic air (20% O_2 in N_2, 99.999% purity, 60 ml min^{-1}), their weight was recorded as a function of temperature. Initial masses were typically 150 mg and heating took place at 10 K min^{-1} to 1073 K (held for 30 min). A correction for the temperature dependence of the buoyancy was performed. Analysis of the reaction products was carried out by means of a quadrupole mass spectrometer. In this way, carbon-containing molecules and fragments could be identified in the off-gas, which assisted in determination of

the thermal range in which oxidation of the organic moieties took place.

Hydrophobicity was assessed from the three-phase contact angle of a water droplet that was deposited on top of a silica flake by means of a fine needle. A specially designed set-up was used, equipped with a goniometer.

Adsorption–desorption isotherms of N_2 (77 K), CO_2 (273 K) and C_2H_2 (273 K) were determined on a CE-Instruments Sorptomatic 1990. All materials were pre-treated by evacuation below 10^{-4} mbar at 473 K. Surface areas were determined from the adsorption isotherms by the Dubinin method, modified by Kaganer,[17] between $p/p^0 = 2 \times 10^{-5}$ and 1×10^{-2}, represented by:

$$\log n = \log n_m + D (\log p^0/p)^2 \quad (1)$$

with n the gas adsorbed at relative pressure p/p^0, n_m the monolayer capacity of the surface, both in mol per g adsorbent, and D an adsorbate-dependent constant. This constant has smaller (more negative) value for smaller pore sizes, and may serve as a check for the actual pore size assessment. Surface areas A were subsequently determined according to

$$A = n_m a_m N_A \quad (2)$$

in which N_A is Avogadro's number and a_m the area occupied by a molecule in the completed monolayer, taken to be 0.162 nm^2 for N_2 (ISO 9277), 0.179 nm^2 for CO_2 and 0.204 nm^2 for C_2H_2. While the surface areas are accurate within a few $m^2\ g^{-1}$, it should be noted that they are an approximation for very small pores with sizes of the order of those of the gas molecules, as an exact surface area can, in principle, only be determined for flat (infinite) surfaces. Ultramicropore (diameter <0.6 nm) sizes were calculated from the ratio of the surface areas determined with the different molecules, taking into account the critical diameters of these molecules for adsorption.[18] Micropore and supermicropore (diameter >1.3 nm)[19] size distributions were determined from the N_2 adsorption isotherms between $p/p^0 = 0$ and 0.2 with the Saito–Foley method,[20] using the adsorption potential for N_2 on a zeolite.[21]

(Bulk) densities of materials were measured by a multivolume Micromeritics 1305 Pycnometer at room temperature using He as replacement gas, and have an accuracy within 1%. The dried samples were flushed with He (99.999% pure) until a sequence of measured volumes remained unchanged. From combination with values found by liquid pycnometry with Hg, total pore volumes v_p were determined with 0.005 $cm^3\ g^{-1}$ accuracy.

High resolution scanning electron microscopy was carried out on a LEO Gemini 1550 FEG-SEM at a voltage of 2.0 kV.

^{29}Si magic angle spinning nuclear magnetic resonance (MAS-NMR) on calcined gels was carried out on a Bruker 300 MHz NMR in a 0.7 mm rotor (0.4 cm^3 of material) with a spinning frequency of 4 kHz. An 8.93 μs pulse was used with a delay of 300 s. Samples were measured during 72 h and deconvolution of the spectra to assess the degree of condensation was carried out with WINNMR.

3. Results

3.1. Thermal stability in dry air

The stability of the organic groups in an oxygen-containing atmosphere was assessed by TGA-MS. Differential weight traces are shown in Fig. 1 for all materials. Mass loss due to decomposition and oxidation of organic groups was assessed by the MS signals of CO_2 and other organic components. This contribution could thus be separated from the mass losses related to dehydration and dehydroxylation, which extend over the whole range from room temperature up to 1073 K. In Table 1, the onset temperature of oxidation is given, *i.e.* the lowest temperature at which weight loss related to organic groups can be observed. Decomposition or pyrolysis did not occur for any of the samples at temperatures below 585 K, while the samples were stable up to at least 673 K in N_2. For the diluted samples, the organic groups were more stable at low MTES concentration, which becomes apparent from the higher onset temperature.

Most samples appeared white after calcination to 1073 K, but blackening was observed for the diluted 25% MTES sample, and to a lesser extent for the 75% and 100% MTES samples. This is likely a sign of slow O_2 transport into the pores, resulting in incomplete oxidation and in decomposition (charring) of organic groups that subsequently remain

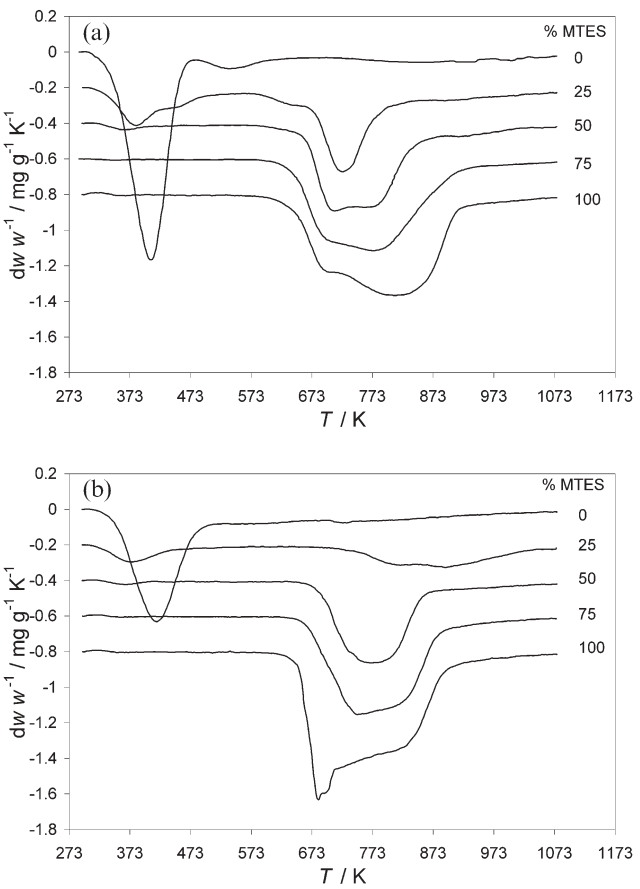

Fig. 1 TGA differential weight traces of silica gels prepared from undiluted (a) and diluted (b) sols. A vertical shift has been applied to separate the traces.

Table 1 Onset and average temperatures (K) of decomposition of organic groups for gels from TEOS–MTES mixtures (synthetic air; $dT/dt = 10$ K min^{-1})

	Undiluted		Diluted	
MTES (mol%)	T_{Onset}/K	$T_{average}$/K	T_{Onset}/K	$T_{average}$/K
25	585	726	680	875
50	585	742	650	762
75	585	757	630	770
100	585	771	590	754

entrapped in the sample. The MS signals of the diluted 25% MTES sample also differed from those of the other samples, in that CH_x fragments were detected prior to CO_2, instead of simultaneously. This signifies that decomposition occurred before oxidation, indicating again very slow transport of oxygen.

In Table 1, the average values of the high-T peaks of Fig. 1 are given, showing lower mean decomposition temperatures for 'undiluted' materials than for 'diluted' materials. As the 'undiluted' samples are thicker, O_2 transport should be slower, which would give a higher decomposition temperature. The difference between undiluted and diluted is least prominent at high MTES concentrations. It is likely that the higher stability of the organic groups in air in the diluted materials is related to a smaller pore size and thus to slower transport of oxygen. The diluted 25% MTES sample showed a very high decomposition temperature and charring, as discussed above, indicating very narrow pores.

3.2. Hydrophobicity and extent of condensation

3.2.1. Ambient water adsorption. A sharp decrease of the weight observed by TGA-MS around 373 K could be attributed to water desorption, and a gradual weight loss over the whole range up to 1073 K to dehydroxylation. In Fig. 2, the weight fraction of adsorbed water is shown, as determined from the weight loss below the onset temperature of oxidation/decomposition. As all samples had been calcined at 673 K, water desorption below this temperature (except for water evolution related to decomposition processes) is due to exposure to ambient air and can be related to the affinity of the material to water vapour. For calcined TEOS, significant re-adsorption of water takes place during storage, while the affinity for water decreases readily by modification. Water adsorption can also be detected for the undiluted 25% MTES sample and is negligible at 50% MTES concentration and higher.

3.2.2. Three-phase contact angle and surface microstructure. A well-established measure of hydrophobicity is the three-phase contact angle with H_2O. However, for many materials the surfaces are too rough to obtain reliable values, and similarly three-phase contact angles cannot be determined with great accuracy for powders.[22] Despite the small size of the flakes, the TEOS–MTES mixtures were sufficiently smooth that accurate and reproducible values could be determined for all samples. A clear relation with the MTES concentration was found, as shown in Fig. 3, and higher values were found for materials prepared from diluted sols. This is in accordance with the TGA data, which indicate smaller water uptakes for materials with high MTES concentrations and for 'diluted' materials. The latter may be explained by a higher degree of condensation (see below) that gives rise to a lower surface density of hydrophilic OH groups.

SEM inspection of a TEOS surface showed surface structures with horizontal dimensions in the order of 0.1–1 μm on the 'diluted' material, which were not found on the 'undiluted' sample. Formation of these structures may be explained by stronger shrinkage during drying of the diluted gel.

3.2.3. MAS-NMR. MAS-NMR spectra of diluted and undiluted 50% MTES materials were found to be visually equal and showed overlapping peaks. By deconvolution of the spectra, values for Q_n and T_n were obtained, *i.e.* the number of Si–O–Si bonds from TEOS and MTES monomers, respectively. From these numbers, the individual and total connectivities C (*i.e.*, the actual number of siloxane bonds per possible bond) were calculated, as given in Table 2. As all remaining groups (except CH_3) consist of OH, we find 5.3% uncondensed Si–OH groups for the undiluted material, and 4.9% for the diluted material. The higher OH surface density of the undiluted material may explain the lower

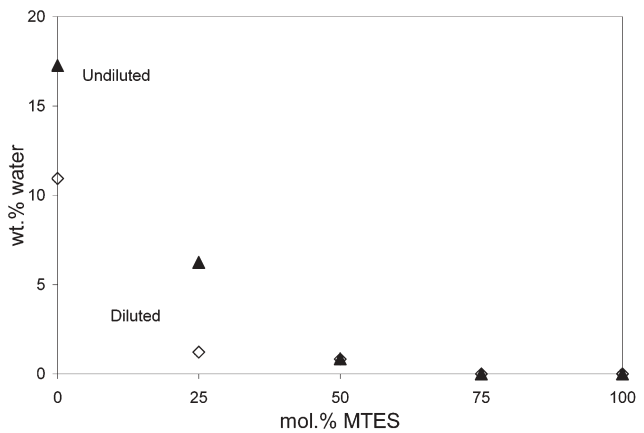

Fig. 2 Weight fraction of adsorbed water determined from TGA-MS. Solid triangles: undiluted; open diamonds: diluted series.

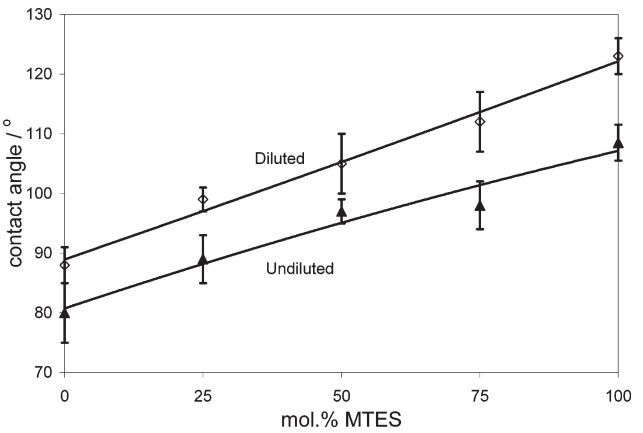

Fig. 3 Three-phase contact angles of water on silica gels from diluted and undiluted sols. The lines serve as a guide to the eye.

Table 2 Number of Si–O–Si bonds per Si atom n for Q (TEOS) and T (MTES) monomers for samples prepared from 50% MTES, along with the Q, T and total connectivity C (actual number of bonds per possible Si–O–Si bond)

	Q_n	C_Q	T_n	C_T	C
Undiluted	3.79	0.948	2.84	0.946	0.947
Diluted	3.88	0.970	2.80	0.932	0.951

hydrophobicity (contact angle) for this sample (see section 3.2.2.). Remarkably, only the Q connectivity is higher for the diluted material. Dilution thus appears to enhance mostly the connectivity of Q (TEOS) monomers and not of the T (MTES) monomers.

3.3. Micropore structure

3.3.1. Adsorption isotherms. Adsorption of N_2, CO_2 and C_2H_2 was carried out on all materials. N_2 isotherms of the silica gels are all of type Ia, characterising microporous materials. The initial parts of the isotherms, relevant for micropore analysis, are shown in Fig. 4. Due to the large differences in adsorption, the isotherms have been normalised in order to allow better comparison. Equilibration times were long (>2 h) for all probe molecules, but especially so for N_2, which has the largest critical diameter (0.3 nm) and is applied at the lowest temperature. The long equilibration times are clearly related to the microporous character of the materials. The longest times were found for both samples from pure TEOS (0% MTES) and for the diluted 25% MTES sample, even at the low relative pressures for CO_2 and C_2H_2 adsorption at 273 K.

For N_2, the surface areas, determined by Dubinin fits from the low-pressure part of the isotherms, vary substantially for the different materials (Table 3). A number of materials are virtually closed towards N_2, while others exhibit very high surface areas. For some materials, the N_2 surface areas are higher than those determined with CO_2 or C_2H_2, despite its large critical diameter. This can be explained in three different ways. The first may be micropore filling, *i.e.*, adsorption of N_2 on the pore surface occurring simultaneously with filling of the pore interior,[23] which does not take place for CO_2 or C_2H_2. This results in overestimation of the N_2 surface areas and only occurs for pores that are at least 3 N_2 molecules wide, *i.e.* approximately 0.9 nm or more. A second explanation for the larger surface areas is a possibly different orientation of N_2 on hydroxylated surfaces, such that it probes a smaller surface and gives a seemingly higher surface area. However, this explanation is only valid for N_2 molecules in the larger pores.[24] Finally, N_2 occupies the smallest volume, although it has the largest critical diameter for passage through a pore opening. While the pore openings may be tight, the volume of the pores may be of such a size that more N_2 fits in than does CO_2 or C_2H_2. Still, considering the first two possible explanations, surface areas determined from the adsorption of CO_2 or C_2H_2 are expected to be more accurate. As the materials are fairly

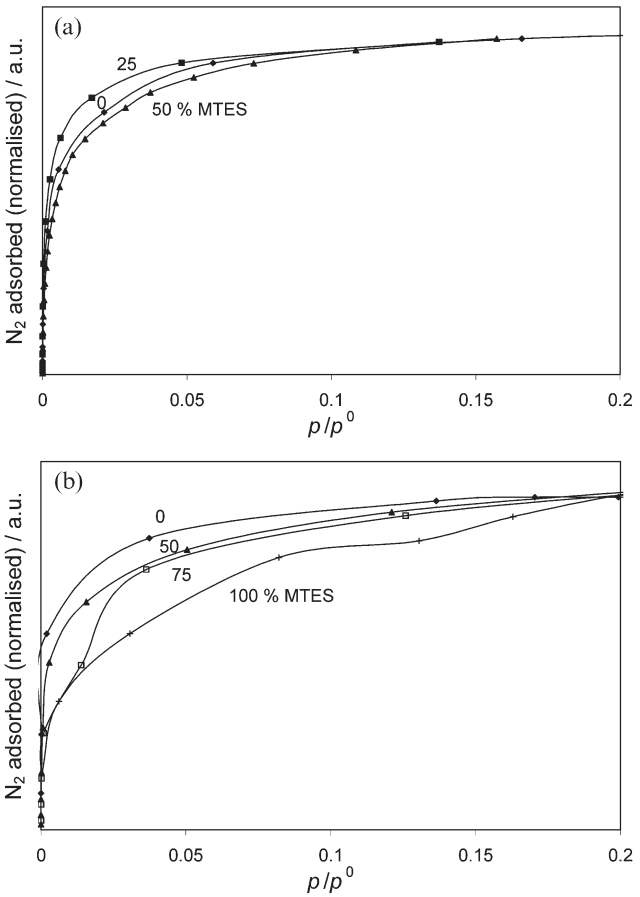

Fig. 4 Initial parts of N_2 isotherms of MTES–TEOS-based gels from undiluted (a) and diluted (b) sols. The isotherms have been normalised for better comparison.

Table 3 Analytical data (N_2, CO_2 and C_2H_2 surface areas, pore volume from He and Hg pycnometry, mean ultramicropore diameters estimated from surface areas, and mean Saito–Foley pore diameters) of gels from undiluted and diluted MTES–TEOS sols

MTES (%)	$A(N_2)/m^2\ g^{-1}$	$A(CO_2)/m^2\ g^{-1}$	$A(C_2H_2)/m^2\ g^{-1}$	$v_p/cm^3\ g^{-1}$	Average d_{ump}/nm	Mean d_p SF/nm
Undiluted						
0	590	509	538	0.100	>0.3	1.50
25	660	272	444	0.091	0.265	1.38
50	478	179	186	0.114	0.278	1.58
75	16	161	242	0.129	0.267	—
100	4	103	285	0.157	0.254	—
Diluted						
0	33	360	261	0.109	0.282	1.33
25	3	175	621	0.119	0.251	—
50	403	155	222	0.127	0.268	1.50
75	159	119	205	0.136	0.263	1.92
100	12	103	211	0.128	0.260	2.04

rigid both at 77 K and at 273 K, we expect no additional hindrance for the passage of N_2 molecules as a result of the lower adsorption temperature, such as observed for modification with a (linear chain) PDMS-like layer.[11]

The CO_2 surface areas show a trend towards smaller values with increasing MTES concentration, while somewhat more complex characteristics are found with C_2H_2. As C_2H_2 has a smaller critical diameter (0.24 nm) than CO_2 (0.28 nm),[18] larger quantities will be adsorbed in small micropores. For pore size distributions or pore entrances with a mean just above the critical diameter of C_2H_2, this will result in a large difference in adsorption between C_2H_2 and CO_2. A similar difference will be found between the surface areas determined with CO_2 and N_2—in the absence of micropore filling—as N_2 in turn has a larger critical diameter (0.3 nm) than CO_2. An estimate of the average ultramicropore size d_{ump} (Table 3) has been obtained from the ratio of the surface areas A_{C2H2} and A_{CO2} measured with the various molecules, and scaling this to the respective critical diameters d_{C2H2} and d_{CO2}:

$$d_{ump} = d_{C2H2} + (d_{CO2} - d_{C2H2})\cdot A_{CO2}/A_{C2H2} \qquad (3)$$

For diluted TEOS, a similar relation has been used with CO_2 and N_2. With increasing MTES concentration, a rough trend can be observed towards smaller pore diameters. Considering the large N_2 surface areas measured for undiluted samples with 25 and 50% MTES and diluted samples with 50 and 75% MTES, these samples must also have larger pores in addition to the smallest ultramicropores. Assuming that micropore filling is responsible for the large N_2 surface areas, the mean diameter of these larger pores will be >0.9 nm.

A check for the validity of ultramicropore sizes is to compare these to the values of D found from the Dubinin fits (Fig. 5). As a stronger dependence of the actual adsorbed amount on the relative pressure is generally found for very small pore sizes, a smaller (more negative) value for D in the fit (eqn (1)) indicates smaller pore sizes. The same trend with MTES concentration can indeed be observed for the estimated pore diameter and for the value of D for CO_2 and C_2H_2. Similarly as for d_{ump}, the 'diluted' 25% MTES material gives D values somewhat off the general trend. This is not the case for 'undiluted' 25% MTES, which may be related to the larger pores that are also present in this material. The D values found with N_2 do not show a clear trend, which can be explained by its large critical diameter as compared to the small pores.

Remarkably, the dependency of d_{ump} on the MTES concentration is much stronger for undiluted materials. In TEOS-rich samples, clearly larger ultramicropores are formed than in diluted samples, which is in accordance with the lower extent of condensation for these monomers, as observed for 50% MTES (see Section 3.2.3 and Table 2). For MTES-rich samples, dilution gives little difference.

3.3.2. Density and pore volume. Bulk densities were measured with a pycnometer. As He (critical diameter 0.2 nm) was used as a replacement gas, the smallest pores could be probed, which is highly relevant for the ultramicroporous materials that are being studied here. However, even with this smallest probe molecule, instant equilibrium was not reached for the thicker materials that were prepared from the undiluted sols. These gels exhibited equilibration times of 1–2 minutes, while those prepared from diluted sols all reached equilibrium within a few seconds. The long equilibration times can be explained well by the ultramicroporous character of the materials. For more bulky materials, transport of the gas into the interior of the particles is limited by the small size of the pores, which is on the order of magnitude of the size of gas molecules. However, for the gel from undiluted TEOS equilibrium was reached quickly as well, which likely indicates that the pore entrances were clearly larger than 0.2 nm (the critical diameter of He).

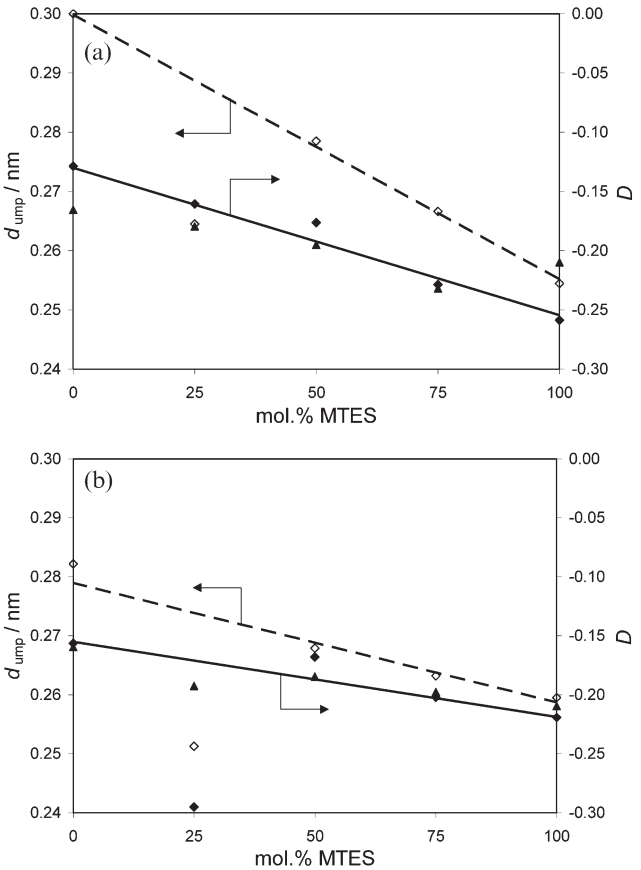

Fig. 5 Ultramicropore diameters (open symbols, dashed trendline) and parameters D (closed symbols) from Dubinin fits of CO_2 (triangles) and C_2H_2 (diamonds, solid trendline) isotherms for gels from undiluted (a) and diluted (b) sols.

In Fig. 6 it can be seen that the density clearly decreases with the extent of organic modification. Lower densities were also found for the 'undiluted' than for the 'diluted' materials, which may be explained by a combination of overestimation of the volume related to slow transport of He to the particle interior, and a somewhat higher hydroxyl surface density. The larger scatter for these materials is another indication that transport limitations play a significant role here. From the lower density of organic polymers (around 1 g cm^{-3}), it can be anticipated that methylated silica also has a theoretically lower density than SiO_2. However, extrapolation of the data would interestingly result in hypothetical zero density for materials with 3 methyl groups per Si (*i.e.* hexamethyldisiloxane, actual density 0.76 g cm^{-3}) and negative density for tetramethylsilane

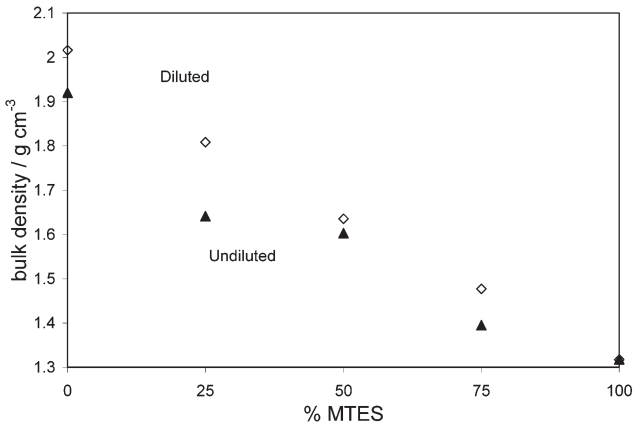

Fig. 6 Bulk densities from volumes determined by He pycnometry. Solid triangles: undiluted; open diamonds: diluted series.

(actual density 0.65 g cm^{-3}). This indicates that the introduction of methyl groups gives rise to a relatively large volume that cannot be probed with He. This is likely created during synthesis from structures formed by 'repulsion' between hydrophobic methyl groups and the remainder of the SiO_2 network. The methyl groups may get directed towards each other, like micelles, and become either inactive (closed) pores, or pore structures that are so small that they can hardly be probed, even with He (<0.2 nm). Such structures may occupy a comparatively large volume and can thus give rise to a smaller measured density.

Particle volumes were determined by liquid Hg pycnometry. Hg encloses the particles but does not intrude into regions with dimensions smaller than about 0.01 mm. By combination of these data with the bulk densities, pore volumes were calculated (Fig. 7). An increase of the pore volume with MTES concentration was observed, as well as somewhat smaller pore volumes for the 'undiluted' series. The latter can be partly related to the slow He transport described above. Moreover, the smaller size of the flaky diluted materials may give rise to a relatively large dead volume, resulting in a higher apparent pore volume.

While the combined CO_2 and C_2H_2 adsorption data indicate a decrease of the pore diameter, a larger pore volume with increasing MTES concentration was calculated, which rather points at a more open structure. This can be explained by the presence of a large number of very small pores in the order of 0.2 nm, such that only molecules as small as He can pass. We thus find that at high MTES concentration small ultramicropores are formed with a distribution that extends down towards sizes below 0.2 nm, part of which cannot be probed.

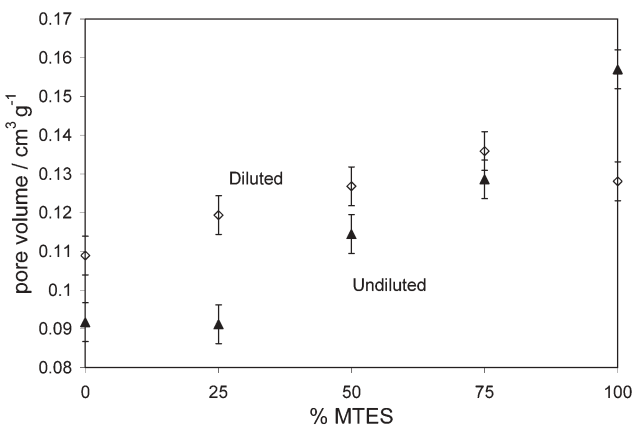

Fig. 7 Pore volumes determined by He and Hg pycnometry. Solid triangles: undiluted; open diamonds: diluted series.

We found generally smaller surface areas for increasing MTES concentration with both N_2 and CO_2, which agrees with the smaller surface areas Da Costa *et al.* found for similar materials, measured with N_2.[15] No changes in pore size were concluded from their data. However, by the use of smaller probe molecules, this appears to be an apparent effect, and we have now obtained evidence that in fact very small pore structures are formed for MTES-modified materials.

3.3.3. Micropore size distribution: Saito–Foley fits. Micropore/supermicropore size distributions were determined by Saito–Foley fits of the N_2 adsorption isotherms, although, due to the comparatively large critical diameter of N_2, adsorption on a number of materials was only very limited and fits could not be made. Still, rough trends can be observed from the fits. It can be seen from Fig. 8 that the diameter of pores with sizes around 1–1.5 nm increases with MTES

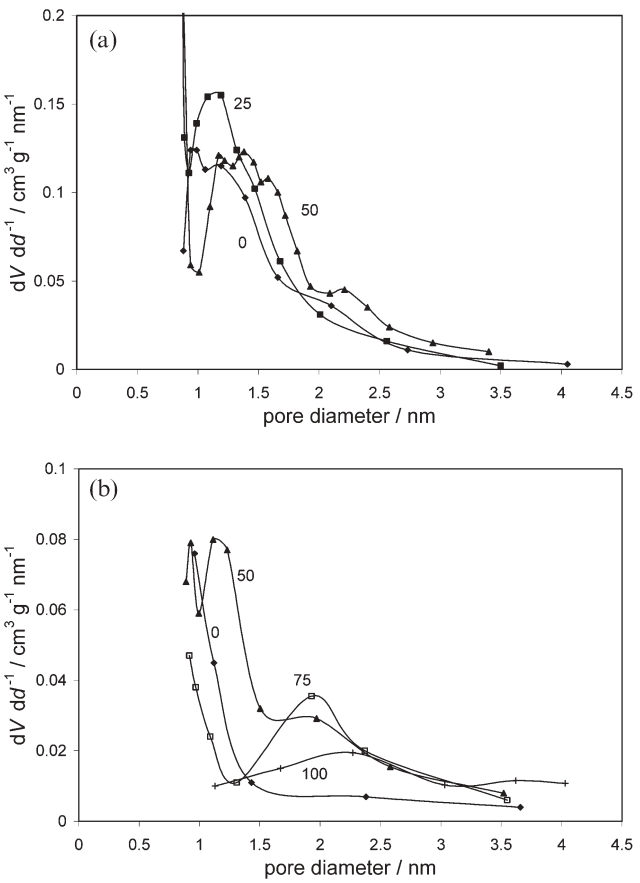

Fig. 8 Saito–Foley fits of of N_2 adsorption isotherms of MTES–TEOS-based silica from (a) undiluted; (b) diluted (0, 100% MTES enlarged 10 times) sols. Diamonds: 0% MTES; solid squares: 25% MTES; triangles: 50% MTES; open squares: 75% MTES; crosses: 100% MTES.

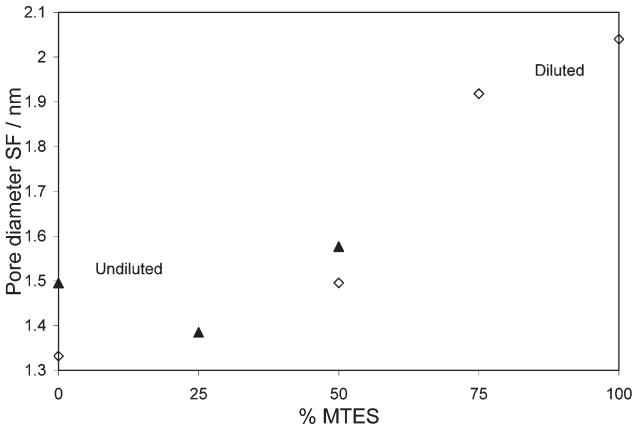

Fig. 9 Mean pore diameters from Saito–Foley fits of N_2 adsorption isotherms of MTES–TEOS-based silica. Solid triangles: undiluted; open diamonds: diluted series.

concentration and that pores with sizes of around 2 nm become more apparent. The latter were also found by Da Costa[15] and give rise to an increase of the mean pore diameter (Fig. 9). These more marked supermicropores thus show a trend opposite to the smaller ultramicropore diameter at higher MTES concentrations estimated from the ratios of the surface areas. Both may be related to the formation of certain stable silsesquioxane-type structures, favoured by 'repulsion' between hydrophilic and hydrophobic parts, as discussed above. These are more prone to form in an early stage for high MTES concentrations and may give rise to both very small pores (<0.3 nm) and pores of around 2 nm. Another explanation for the formation of such structures may be the lower number of condensable groups in MTES. It can be presumed that the larger pores facilitate transport of gas molecules towards the smaller pores, thus allowing somewhat faster equilibration for adsorption of C_2H_2, CO_2 and N_2, as observed for samples with 50% and more MTES. Longer equilibration times for adsorption of gas molecules for samples with 0% and (diluted) 25% MTES could similarly indicate the absence of a large fraction of supermicropores. The fast He transport for the thicker (undiluted) pure TEOS sample on the other hand indicates that no structures with pore sizes of around 0.2 nm have been formed, while slower He transport in the 'undiluted' MTES-containing samples may indicate the abundant presence of such very small pore structures. The pore size distribution of materials prepared from pure TEOS is thus more uniform. The presence of 2 nm supermicropores in an ultramicroporous structure indicates a bimodal pore size distribution for MTES-containing materials. Although the actual values of the pore diameters may differ somewhat in supported films, this could also explain why a membrane prepared with 50% MTES exhibits a somewhat lower selectivity than a membrane from pure TEOS.[12]

4. Conclusions

Co-condensation of TEOS with MTES gives rise to more hydrophobic materials with a significantly lower affinity to water. The organic groups are highly stable in an oxidative atmosphere up to at least 585 K. Water adsorption from ambient air becomes negligible for materials based on 50% MTES or more. Sols that were diluted prior to gelation and ageing also showed a higher hydrophobicity, which we could relate to a higher degree of condensation and a corresponding lower OH density observed by MAS-NMR. For mixed materials with 50% MTES, the connectivity of only the TEOS monomers was higher. The higher overall hydrophobicity is most likely the result of more effective drying/dehydroxylation during calcination of the much thinner 'diluted' materials. The tunable enhanced hydrophobicity indicates that it will be worthwhile to further assess the long-term structural stability under wet conditions.

Gels prepared from a combination of TEOS and MTES showed smaller ultramicropore sizes, down to 0.2 nm diameter, with increasing MTES concentration, as determined from adsorption of various probe molecules with different critical diameters. The total pore volume increased with MTES concentration, which can predominantly be attributed to very small pores of around 0.2 nm. In addition, the bulk density sharply decreased with MTES concentration, indicating the presence of a large number of closed pores or regions with sizes below 0.2 nm that cannot be probed even with He. Dilution had only a minor effect on the structure of gels from pure MTES, while clearly smaller pores were found upon dilution in cases where TEOS was also present in the initial sol.

A similar difference with MTES concentration was found from oxidation/decomposition of the organic groups, which was at higher temperatures only for 'diluted' materials with low MTES concentration, indicating pores that are less open towards transport of O_2 and oxidation products. The results indicate that denser structures are formed for diluted materials by more extensive condensation of TEOS species, which can be related to more effective heating of these thinner materials. Moreover, it can be envisaged that the smaller pore size is the result of more controlled formation of a dense network structure due to the lower reaction kinetics during gelation and ageing, and longer duration of these steps. It is thus likely that by dilution a more intimate mixture is formed. A material based on 25% MTES showed particularly small pore sizes, which may be related to very effective mixing, but no indications were found of the smallest pore structures that were observed at high MTES concentration.

In addition to the ultramicropores, some supermicroporosity was observed, which gives rise to micropore filling with N_2 for some materials. Besides, pores with sizes of around 2 nm were observed for gels with large MTES concentration. These supermicropores may facilitate transport of gas molecules towards the ultramicropores. As there is a growing interest in materials with such bimodal pore size distributions for reasons of higher diffusion rates, the class of materials investigated here may be particularly promising. For TEOS-rich gels, the number of supermicropores was very small and the pore size was more homogeneous, which also explains the somewhat higher selectivity of membranes from pure TEOS. It was postulated that both very small pores down to below 0.2 nm, and pores with sizes around 2 nm, are formed as a result of the presence of silsesquioxane-type structures in a sol with MTES. Such highly stable structures are likely formed in an early stage of preparation, related to repulsion between

hydrophobic (methyl groups) and hydrophilic parts as well as to the fast hydrolysis of MTES. This would also explain why dilution during gelation has little effect on the pore structure in gels prepared from pure MTES. The homogeneity of mixing of the different precursors is high even on a microscopic level, as found from the low affinity to water for gels from TEOS–MTES mixtures. The tunability of both the hydrophobicity and the pore size provides good prospects for further development of methylated silica in molecular separation applications.

Acknowledgements

The authors thank Mark A. Smithers of the MESA+ Institute for Nanotechnology for the high-resolution SEM measurements, Wim Genuit of Shell Research and Technology Centre Amsterdam for carrying out MAS-NMR measurements and Johan C. Groen of the Delft University of Technology for practical assistance with 3-phase contact angle measurements. Jaap F. Vente, Paul P. A. C. Pex, and members of the Energy Efficiency in the Industry group of the Energy Research Centre of the Netherlands are acknowledged for fruitful discussions. This research is supported by the Netherlands Technology Foundation STW, applied science division of NWO and the technology programme of the ministry of economic affairs.

References

1 J. J. Ebelmen, *C. R. Hebd. Seances Acad. Sci.*, 1844, **19**, 398; J. J. Ebelmen, *Ann. Chim. Phys.*, 1846, **16**, 129; J. J. Ebelmen, *J. Pharm. Chim.*, 1844, **6**, 262.
2 W. A. Patrick, *US Pat.* 1297724, 1919.
3 R. J. R. Uhlhorn, M. H. B. J. Huis in't Veld, K. Keizer and A. J. Burggraaf, *J. Mater. Sci. Lett.*, 1989, **8**, 1135.
4 A. Larbot, A. Julbe, C. Guizard and L. Cot, *J. Membr. Sci.*, 1989, **44**, 289.
5 A. W. Dearing and E. E. Reid, *J. Am. Chem. Soc.*, 1928, **50**, 3058.
6 R. M. De Vos and H. Verweij, *Science*, 1998, **279**, 1710; R. M. De Vos and H. Verweij, *J. Membr. Sci.*, 1998, **143**, 37; F. P. Cuperus and R. W. van Gemert, *Sep. Purif. Technol.*, 2002, **27**, 225.
7 J. Campaniello, C. W. R. Engelen, W. G. Haije, P. P. A. C. Pex and J. F. Vente, *Chem. Commun.*, 2004, 834.
8 R. K. Iler, *The Chemistry of Silica*, Wiley & Sons Inc., New York, USA, 1979.
9 L. T. Zhuravlev, *Colloids Surf., A*, 2000, **173**, 1.
10 L. R. Snyder and J. W. Ward, *J. Phys. Chem.*, 1996, **70**, 3941.
11 H. L. Castricum, M. C. Mittelmeijer-Hazeleger, A. Sah and J. E. ten Elshof, *Microporous Mesoporous Mater.*, 2006, **88**, 63.
12 R. M. De Vos, W. F. Maier and H. Verweij, *J. Membr. Sci.*, 1999, **158**, 277.
13 M. Pauthe, F. Despetis and J. Phalippou, *J. Non-Cryst. Solids*, 1993, **155**, 110; H. Yokogawa and M. Yokoyama, *J. Non-Cryst. Solids*, 1995, **186**, 23; C. Della Volpe, S. Dirè and E. Pagani, *J. Non-Cryst. Solids*, 1997, **209**, 51; S. Dirè, E. Pagani, F. Babonneau, R. Ceccato and G. Carturan, *J. Mater. Chem.*, 1997, **7**, 67; S. Dirè, E. Pagani, R. Ceccato and G. Carturan, *J. Mater. Chem.*, 1997, **7**, 919; T. Takei, A. Yamazaki, T. Watanabe and M. Chikazawa, *J. Colloid Interface Sci.*, 1997, **188**, 409.
14 M. J. van Bommel, T. N. M. Bernards and A. H. Boonstra, *J. Non-Cryst. Solids*, 1991, **128**, 231.
15 J. C. D. Da Costa, G. Q. Lu and V. Rudolph, *Colloids Surf., A*, 2001, **179**, 243.
16 R. S. A. De Lange, J. H. A. Hekkink, K. Keizer and A. J. Burggraaf, *J. Membr. Sci.*, 1995, **99**, 57.
17 M. G. Kaganer, *Zh. Fiz. Khim.*, 1959, **33**, 2202; S. J. Gregg and K. S. W. Sing, *Adsorption, Surface Area and Porosity*, Academic Press, London, 2nd edn, 1982, p. 42.
18 M. C. Mittelmeijer-Hazeleger, H. De Jonge and A. Bliek, in *Characterization of Porous Solids IV*, ed. B. McEnaney, T. J. Mays, J. Rouquérol, F. Rodriguez-Reinoso, K. S. W. Sing and K. K. Unger, The Royal Society of Chemistry, Cambridge, UK, 1996, p. 429.
19 M. M. Dubinin, *J. Colloid Interface Sci.*, 1974, **46**, 351.
20 A. Saito and H. C. Foley, *Microporous Mater.*, 1995, **3**, 531.
21 S. Ross and J. P. Olivier, *On Physical Adsorption*, Wiley and Sons, New York, 1964.
22 D. A. Spagnolo, Y. Maham and K. T. Chuang, *J. Phys. Chem.*, 1996, **100**, 6626.
23 K. S. W. Sing, *Colloids Surf., A*, 2001, **187–188**, 3.
24 J. Rouquerol, F. Rouquerol, C. Pérès, Y. Grillet and M. Boudellal, in *Characterization of Porous Solids*, ed. S. J. Gregg, K. S. W. Sing and H. F. Stoeckli, London Society of Chemical Industry, London, 1979, p. 107; J. Rouquerol, F. Rouquerol, Y. Grillet and M. J. Torralvo, in *Fundamentals of Adsorption*, ed. A. L. Meyer and G. Belfort, Engineering Foundation, New York, 1984, p. 501.